Supporting Information for Lattice Mismatch Drives Spatial Modulation of Corannulene Tilt on Ag(111)

Anu Baby,[†] He Lin,[†,#] Abhilash Ravikumar,[†] Carla Bittencourt,[‡] Hermann A. Wegner,[¶] Luca Floreano,[*,§] Andrea Goldoni,[*,‖] and Guido Fratesi[*,⊥]

[†]*Università degli Studi di Milano-Bicocca, Dipartimento di Scienza dei Materiali, via Cozzi 55, I-20125, Milano, Italy*

[‡]*Chimie des Interactions Plasma-Surface, University of Mons, 20 Place du Parc, 7000 Mons, Belgium*

[¶]*Institute of Organic Chemistry, Justus Liebig University Giessen, Heinrich-Buff-Ring 17, 35392 Giessen, Germany*

[§]*CNR-IOM, Laboratorio TASC, Basovizza SS-14, Km 163.5, I-34149 Trieste, Italy*

[‖]*Elettra Sincrotrone Trieste, s.s. 14 km 163.5 in Area Science Park, 34149 Trieste, Italy and INSTM - Elettra, Lab. Micro & Nano-Carbon, s.s. 14 km 163.5 in Area Science Park, 34169 Trieste, Italy*

[⊥]*Dipartimento di Fisica, Università degli Studi di Milano, via Celoria 16, I-20133, Milano, Italy*

[#]*Current address: Institute of Applied Chemistry, Xinjiang University, Urumqi, 830046 Xinjiang, P. R. China*

E-mail: floreano@iom.cnr.it; andrea.goldoni@elettra.eu; guido.fratesi@unimi.it

STM topography of the clean sample

The scale length of the STM images has been calibrated by measuring the clean Ag(111) surface with atomic resolution. We obtained a self-consistent calibration factor at length scales ranging from 3 to 15 nm (largest scale where single atoms could be individually resolved), as shown in the representative images of Figure S1. We recorded a maximum spread of ~ 2 % between horizontal and vertical scanning lengths.

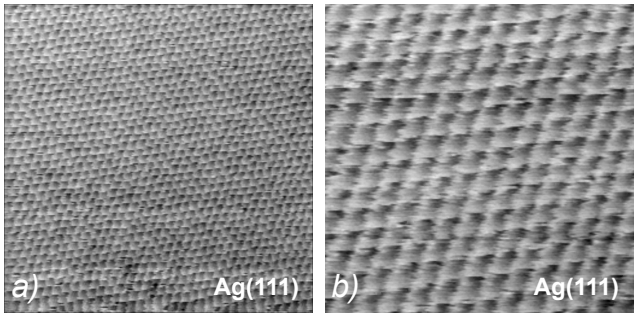

Figure S1: STM topography of the clean Ag(111) substrate: (a) image size $= 10 \times 10$ nm^2 sample bias $= +0.09$ V, $I = 1$ nA; (b) image size $= 3.5 \times 3.5$ nm^2, sample bias $= +0.14$ V, $I = 1.2$ nA. The peculiar contrast is likely due to an unidentified small molecule attached to the STM tip while scanning the sample.

STM topography in the submonolayer range

We observed a very high molecular mobility at room temperature, which prevented the imaging of individual molecules in the submonolayer range. Measurements at the 0.3-0.4 ML coverage revealed the preferential condensation of molecules at step edges that are decorated by fuzzy molecular rows (as shown in Figure S2). Remarkably, the appearance of the fuzzy rows depends on the tip interaction time, where the best molecular definition is achieved at the fastest scanning speed (compare Fig. S2b and Fig. S2c). Both the molecular rows and the step edges are very mobile and change their shape scan after scan (Fig. S2c-d), indicating an interaction of molecules with the steps (and the STM tip) relatively larger than with the substrate. We observed wavy patterns surrounding also local defects (e.g. small holes, clusters and residual contaminants) with the modulation intensity fading away

from them and easily perturbed when trying to zoom in with the STM (Fig. S2e-f). We also attribute this effect to a residential time of molecules at defects larger than on terraces. Similar features were previously reported to surround coronene molecules on Ag(111) and attributed to Friedel-like oscillations induced by the scattering/interference of the Ag Fermi electrons with the molecular orbitals.[1] However this explanation seems not plausible because i) the wavy patterns are not stationary, ii) the intensity oscillations display a transverse modulation of $\sim 10 - 11$ Å that is much larger than the Ag(111) half Fermi wavelength ($\sim 3.8 \pm 0.1$ Å),[2–4] iii) the STM images have been acquired at large bias (> 1 eV), where any contribution from Fermi electrons is smeared out by integration on multiple states of different wavelength,[5] and iv) the images have been acquired at room temperature, where the Fermi electron coherence is strongly reduced.[6] Individual molecules on terraces can be detected only at the saturation of the monolayer, when they are self-assembled into close compact domains oriented along the main symmetry directions (see the main text).

Restructuring of edges of small vacancy islands

Molecules within small vacancy islands display a lower mobility and we could image the step edge restructuring due to the interaction with diffusing molecules, as shown in the sequence of images of Figure S3 taken in the most common case of an hexagonal island (also see the STM movie at 10-12 sec/frame in the Supporting Information). For comparison, we also show the specific case of the triangular vacancy island displaying a static molecular organization.

LEED from the (3×3) reconstruction.

The three-fold diffraction pattern in LEED is observed from ∼50 to ∼21 eV electron kinetic energetic, and becomes the only visible one at the lowest energy (see Figure S4). Apart from more complex dependence of the LEED I-V pattern, the doubling of the escape depth at the lowest energy (from 5 to 10 Å) suggests that the three-fold pattern may be associated with

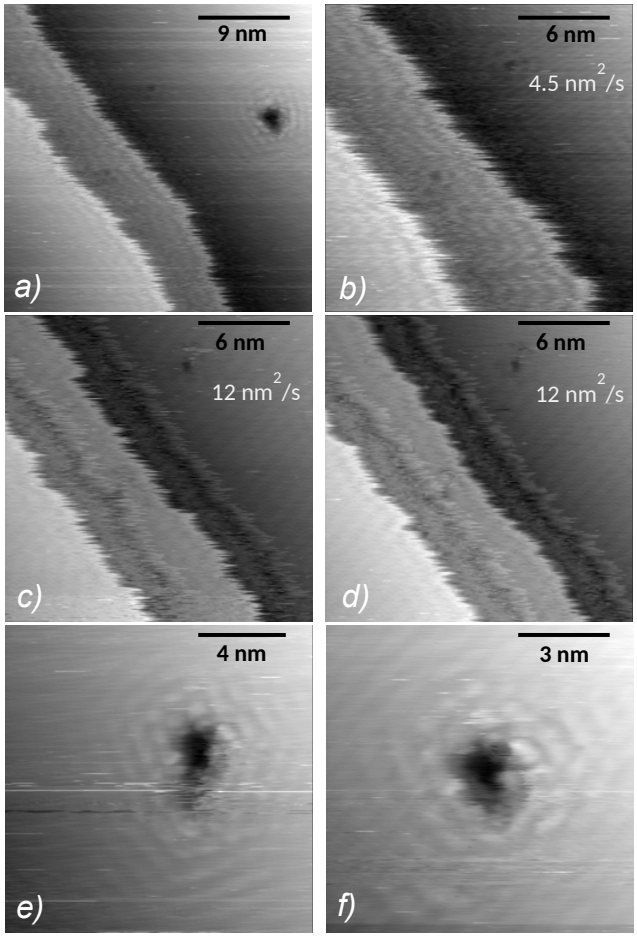

Figure S2: Experimental STM showing step and defect decoration by corannulene at a coverage of 0.3-0.4 ML. All images have been measured with the same sample bias = +1.16 V, and $I = 140$ pA. Panels (a-b): step edges are decorated by molecular rows displaying a fuzzy contrast due to fast mobility, molecules are also decorating isolated defects, such as the small hole formed by tip indentation on the lower terrace. Panels (c-d): consecutive images showing the time evolution of both steps and molecular rows ($\sim$ 25 sec/frame). Panels (e-f): consecutive images showing the time change of the edge of a small defect formed by tip indentation and the vanishing of the surrounding molecules when zooming in with the STM ($\sim$ 20 sec/frame).

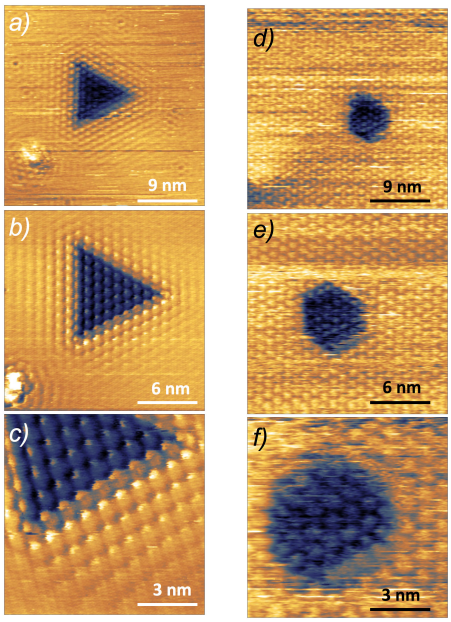

Figure S3: Panels (a-c): images taken at a coverage of 0.3-0.4 ML with scanning areas of increased magnification, sample bias = +1.4 V, $I = 160$ pA; molecules inside the triangular vacancy islands are trapped in a static configuration displaying an intermolecular spacing of 10.5 Å. Panels (d-f): consecutive images taken with ~ 30 sec time laps (~ 10 sec/frame) at a full monolayer coverage with scanning areas of the same size as in (a-c), sample bias= +1.4 V, $I = 450$ pA; the step edges of the hexagonal vacancy island display a fast restructuring.

a reconstruction of the substrate and not only with the local ordering of the corannulene overlayer.

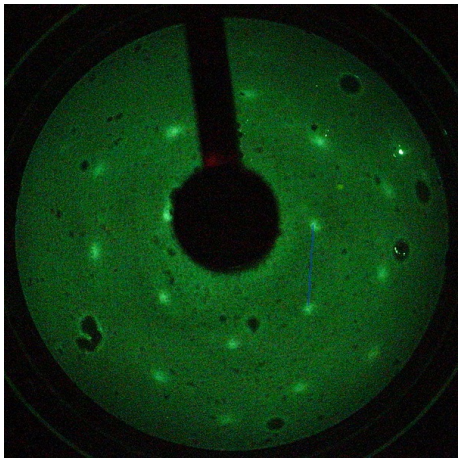

Figure S4: LEED pattern measured at a kinetic energy of 21 eV on the same surface of Fig. 4. The three-fold diffraction pattern is fully developed, without further diffraction spots.

DFT energetics of (3×3) and (4×4) phases

The energy and structural paramenters of (3×3) and (4×4) phases are reported in Table S1 and Table S2, respectively.

Table S1: Computed adsorption energies E_{ads} and azimuthal/tilt angles (ϕ/θ) of (3×3)-corannulene/Ag(111) with ϕ_0 denoting the initial value in the optimization.

	Site	ϕ (°)	θ (°)	E_{ads} (eV)
$\phi_0 = 30°$	B	31.1	30.8	−1.53
	F	30.1	28.0	−1.51
	H	29.9	28.0	−1.51
	T	30.0	33.4	−1.47
$\phi_0 = 15°$	B	10.5	29.6	−1.47
	F	10.4	29.5	−1.49
	H	11.1	30.0	−1.50
	T	6.6	31.4	−1.43

Table S2: Computed adsorption energies E_{ads} as a function of the tilt angle ϕ for flat-lying (4×4)-corannulene/Ag(111). For each adsorption site, the last row reports the the spread in the computed values.

ϕ (°)	FCC (eV)	HCP (eV)	Bridge (eV)	Top (eV)
0	−1.648	−1.660	−1.650	−1.538
15	−1.660	−1.647	−1.654	−1.538
30	−1.661	−1.647	−1.649	−1.538
45	−1.647	−1.660	−1.650	−1.539
60	−1.647	−1.660	−1.653	−1.538
75	−1.647	−1.659	−1.650	−1.538
90	−1.659	−1.659	−1.637	−1.538
105	−1.660	−1.660	−1.649	−1.538
$E_{\mathrm{ads}}^{\mathrm{Max}} - E_{\mathrm{ads}}^{\mathrm{Min}}$ (eV)	0.013	0.013	0.016	0.001

XPS and NEXAFS simulations for gas phase corannulene

As a comparison to spectra for adsorbed molecules reported in the main text, here we present the spectra computed for gas phase molecules. In particular, Figure S5 and Table S3 report the XPS spectra and CLSs computed for the gas phase molecule (black dashed-dotted line in the figure). We can observe that the relative order of the binding energies ($\mathrm{BE_{C1}} < \mathrm{BE_{C3}} < \mathrm{BE_{C2}}$) is the same as upon adsorption. The C1 and C3 peaks are more separated in the gas phase which results in a shoulder-like feature at the high binding energy side. Our results on the relative binding energies, based on the optB88-vdW functionals, are further confirmed by comparing them with an additional calculation with the PBE0 hybrid functional[7] for gas phase molecules: the differences in CLS between the two approaches is no larger than ~ 0.06 eV.

Table S3: Calculated C 1s core level shifts of gas phase and adsorbed corannulene. See Figure S5 for the definition of C1, C2, and C3 species. Adsorbed results in the tilted (3×3) phase are averaged among the atoms in the group.

Species	gas CLS (eV)	(3×3) CLS (eV)	(4×4) CLS (eV)
C1	−0.348	−0.169	−0.141
C2	+0.050	+0.307	+0.231
C3	+0.248	−0.069	−0.045
C2−C3	+0.198	+0.376	+0.276

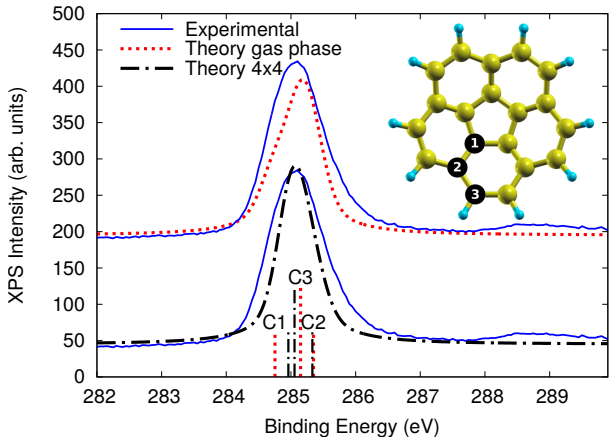

Figure S5: XPS spectrum of corannulene measured for 1 ML on Ag(111) with photon energy $h\nu = 515$ eV (blue solid line), compared to the simulated ones in the gas phase (red dotted line, stacked for clarity) and flat-lying molecules in the (4×4) phase (black dash-dotted line). Vertical sticks show the average contributions from the three groups of C atoms as numbered in the inset. The theoretical spectrum is obtained by broadening the individual C contributions with a pseudo-Voigt profile (50% Gaussian plus 50% Lorentzian both having full width at half maximum of 0.5 eV), and have been aligned to 285.10 eV.

Next, we consider the NEXAFS spectrum for a gas phase molecule reported in Figure S6 Here we presents separately results for the electric field along the molecular axis perpendicular to the central pentagon (panel a, corresponding to p-polarization) and orthogonal to it (panel b, corresponding to s-polarization), although gas phase results would only access the rotational averages. These simulations provide a benchmark corresponding to the hypothetical spectrum of a flat-lying molecule in absense of interaction with the surface. Remarkably, the spectrum is only weakly perturbed by adsorption when comparing simulations for gas phase and flat adsorbed molecules in the (4×4) phase.

Half-core-hole vs full-core-hole NEXAFS spectra

Taking free corannulene as a reference, we compare in Figure S7 our NEXAFS spectra computed by the half-core-hole (HCH) approximation to additional calculations within the full-core-hole (FCH) method. Notice the overly amplified intensity of the LUMO feature ($\approx 284.5 - 285$ eV) over the LUMO+2/ + 3 ones (≈ 286.4 eV).

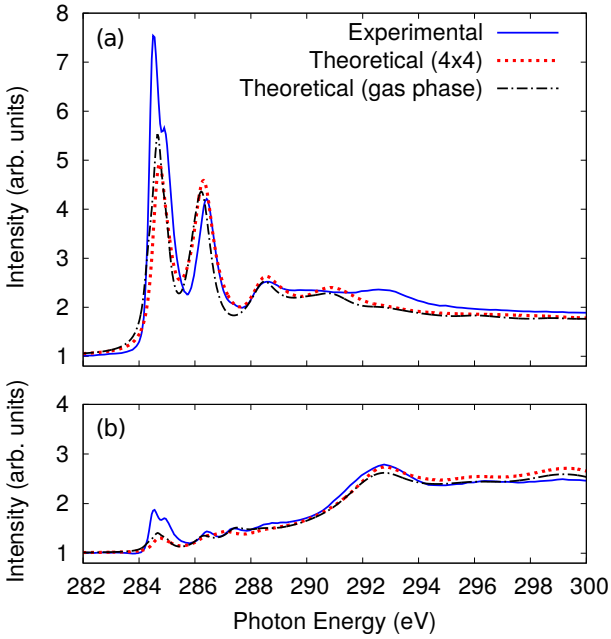

Figure S6: Computed gas phase corannulene NEXAFS spectra for (a) p-polarization and (b) s-polarization compared to simulations for flat-lying (4×4)-corannulene/Ag(111) and measurements at 1 ML coverage. The theoretical spectra are aligned to the experimental LUMO features (data shifted by 284.55 eV and 289.35 eV for adsorbed and free molecules, respectively, giving the different energy reference in the calculation without the substrate).

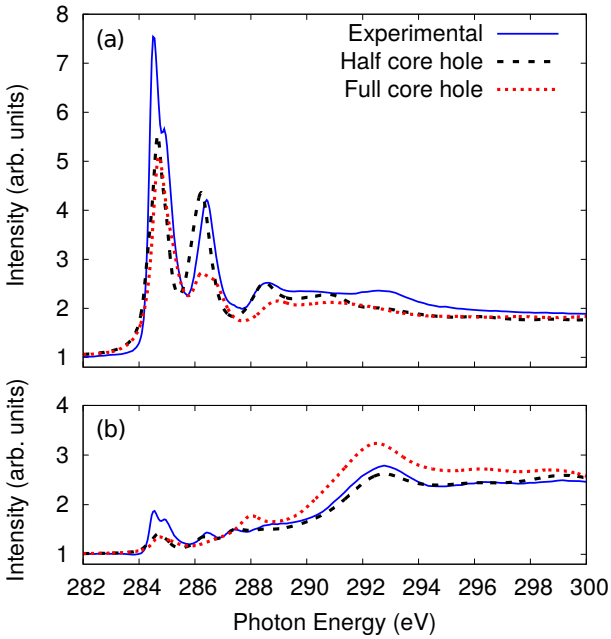

Figure S7: Simulated NEXAFS spectra of gas phase corannulene with half-core-hole and full-core-hole potentials, compared to measurements for 1 ML of corannulene/Ag(111).

Analysis of initial/final-state effects in NEXAFS simulations for gas phase corannulene

The close resemblance of the simulated gas phase spectrum with the adsorbed one further allows a detailed identification of the molecular transitions involved in this simpler case. We follow here the same methodology as in our previous works.[8,9] To gain more insight on the NEXAFS spectra explicit calculation of a few unoccupied states for the free molecule was done on the half positively charged molecule (corresponding to the half-core-hole Hamiltonian used in evaluating the spectra) to identify the molecular orbitals involved in specific transitions at the lower energies. These orbitals were eventually projected onto the ones of corannulene in the ground state[10] to highlight the modification of the electronic structure by the core hole. It is useful to recall the molecular orbitals of ground state corannulene in the gas phase, which have been computed at the Kohn-Sham PBE level and are shown in Figure S8. Their eigenvectors and Kohn-Sham eigenvalues are comparable to the ones in the literature.[11] Interestingly, the LUMO and LUMO+1 states are degenerate, as well as LUMO+4 and LUMO+5 (also HOMO and HOMO-1 are degenerate, although this is less relevant for the current discussion). The lowest-lying state with σ symmetry is the LUMO+6 which involves the C-H bonds.

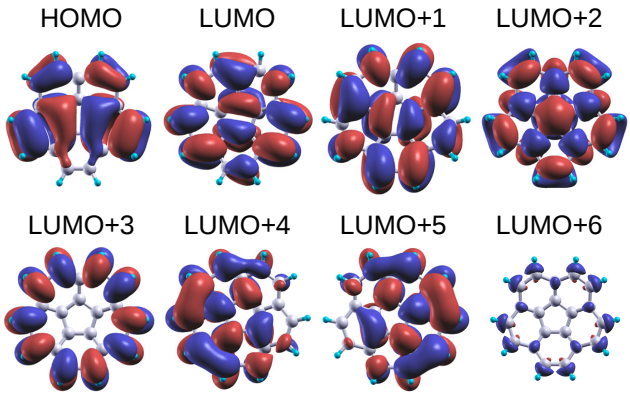

Figure S8: Molecular orbitals of gas phase corannulene. LUMO/LUMO+1 and LUMO+4/LUMO+5 are degenerate.

We report the simulated NEXAFS spectra for the inequivalent C1, C2, and C3 species in

Figures S9(a), (b), and (c), respectively, separating the different initial states and applying a smaller broadening of the spectra to better identify the features. There, we can see that all C species contribute to the first two peaks visible in p-polarization. The first one involves as a final state a molecular orbital which was computed with the half-core-hole and is mostly described in terms of ground state LUMO and LUMO+1 orbitals combined so as to maximize the amplitude on the excited atom; these states are reported in Figure S9 with labels as "Cn-LUMO" (where we indicate by Cn the atom with the core hole). As can be seen in Figure S9, the 1s→LUMO contribution by C3 atoms is at an energy intermediate between those of C1 and C2. This yields to a more structureless feature in the simulated spectrum for gas phase molecules than for adsorbed ones, where C1 and C3 contributions appear at similar energy well distinguished from that of C2 (more similarly to the experiments), see Figure S6). The orthogonal combination of LUMO and LUMO+1, which vanishes at Cn, bears no contribution to the spectrum. Hence the next peak is given by higher orbitals: for C1, by the excited C1-LUMO+3 shown in Figure S9, where we notice that this derives from a combination of the ground state LUMO+4/+5; for C2 and C3, by the excited C2-LUMO+2 and C3-LUMO+2, where the five-fold symmetry of the unperturbed LUMO+2 can still be recognized. The third feature (≈288.6 eV), which is much sharp in the theoretical spectrum in p-polarization, is instead mainly given by the C2 carbon atom, where it results from transition to two molecular orbitals, namely the C2-LUMO+11 and C2-LUMO+12 (see Figure S9). A relatively lower contribution by similar orbitals is also seen for the C1 and C3 atoms. Moving next to the NEXAFS simulated for the s-polarization, we can still see the signature of most structures considered so far, as the molecule is not perfectly planar. However, the first truly σ^* orbital corresponds to the C3-LUMO+6 depicted in Figure S9, and relates to the C-H bond for the excited C3 atom that is however not clearly visible in the spectrum of adsorbed molecules as discussed in the main text.

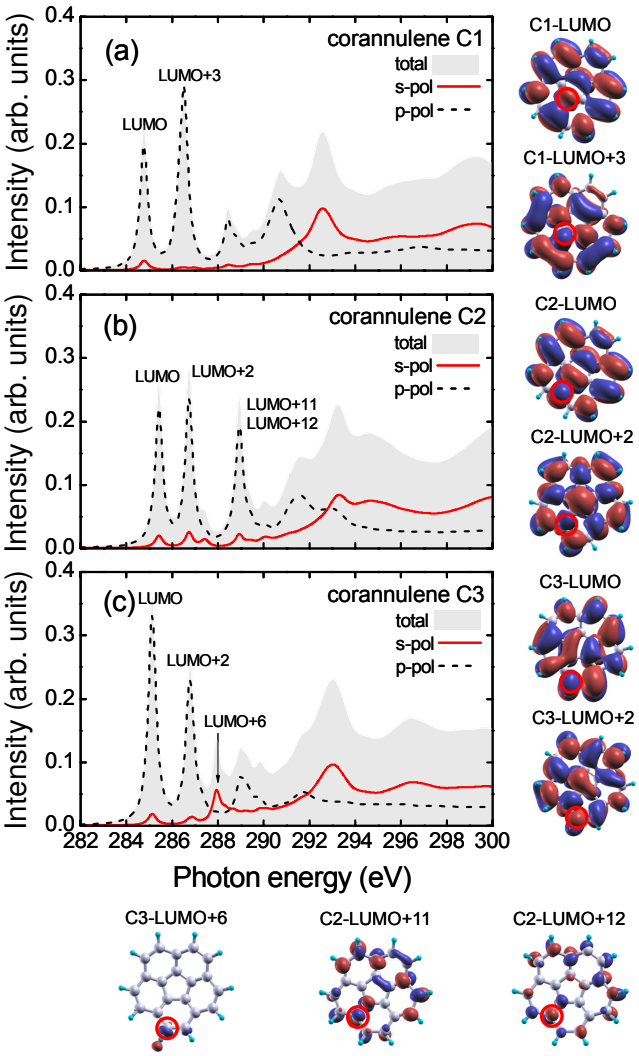

Figure S9: Panels (a), (b), and (c) show the contributions to the NEXAFS spectrum computed for the inequivalent C1, C2, and C3 species, respectively. The gray shaded area marks 3× the average contribution, whereas the black dashed line correspond to the spectrum taken in p-polarization and the red solid line to that in s-polarization. On the right we depict the final-state orbitals for the first two spectral features, computed with the half-core-hole at the atom indicated with the red circle. The bottom line depicts, from left to right: the LUMO+6 orbital contributing to the σ^* peak from C3; the LUMO+11 and LUMO+12 producing the overly sharp peak at 288.6 eV in the spectrum from C2. The theoretical spectra are shifted in energy to match experimental ones.

References

(1) Lackinger, M.; Griessl, S.; Heckl, W. M.; Hietschold, M. Coronene on Ag(111) Investigated by LEED and STM in UHV. *J. Phys. Chem. B* **2002**, *106*, 4482–4485.

(2) Morgenstern, K.; Braun, K.-F.; Rieder, K.-H. Surface-State Depopulation on Small Ag(111) Terraces. *Phys. Rev. Lett.* **2002**, *89*, 226801.

(3) Hla, S.-W.; Braun, K.-F.; Wassermann, B.; Rieder, K.-H. Controlled Low-Temperature Molecular Manipulation of Sexiphenyl Molecules on Ag(111) Using Scanning Tunneling Microscopy. *Phys. Rev. Lett.* **2004**, *93*, 208302.

(4) Kulawik, M.; Rust, H. P.; Heyde, M.; Nilius, N.; Mantooth, B. A.; Weiss, P. S.; Freund, H. J. Interaction of CO Molecules With Surface State Electrons on Ag(111). *Surf. Sci. Lett.* **2005**, *590*, L253–L258.

(5) Li, J.; Schneider, W.-D.; Berndt, R. Local Density of States from Spectroscopic Scanning-Tunneling-Microscope Images: Ag(111). *Phys. Rev. B* **1997**, *56*, 7656–7659.

(6) Hasegawa, Y.; Avouris, P. Direct Observation of Standing Wave Formation at Surface Steps Using Scanning Tunneling Spectroscopy. *Phys. Rev. Lett.* **1993**, *71*, 1071–1074.

(7) Adamo, C.; Barone, V. Toward Reliable Density Functional Methods without Adjustable Parameters: The PBE0 Model. *J. Chem. Phys.* **1999**, *110*, 6158–6170.

(8) Fratesi, G.; Lanzilotto, V.; Stranges, S.; Alagia, M.; Brivio, G. P.; Floreano, L. High Resolution NEXAFS of Perylene and PTCDI: a Surface Science Approach to Molecular Orbital Analysis. *Phys. Chem. Chem. Phys.* **2014**, *16*, 14834–14844.

(9) Baby, A.; Lin, H.; Brivio, G. P.; Floreano, L.; Fratesi, G. Core-Level Spectra and Molecular Deformation in Adsorption: V-Shaped Pentacene on Al(001). *Beilstein J. Nanotechnol.* **2015**, *6*, 2242–2251.

(10) Ravikumar, A.; Baby, A.; Lin, H.; Brivio, G. P.; Fratesi, G. Femtomagnetism in Graphene Induced by Core Level Excitation of Organic Adsorbates. *Sci. Rep.* **2016**, *6*, 24603.

(11) Noguchi, Y.; Sugino, O. Symmetry Breaking and Excitonic Effects on Optical Properties of Defective Nanographenes. *J. Chem. Phys.* **2015**, *142*, 064313.